On the rate sensitivity in discrete dislocation plasticity

Agnihotri, Prabhat; van der Giessen, Erik

Published in:
Mechanics of Materials

DOI:
10.1016/j.mechmat.2015.01.009

Mechanics of Materials 90 (2015) 37–46

Contents lists available at ScienceDirect

Mechanics of Materials

journal homepage: www.elsevier.com/locate/mechmat

On the rate sensitivity in discrete dislocation plasticity

Prabhat K. Agnihotri [a,b], Erik Van der Giessen [a,*]

[a] Zernike Institute for Advanced Materials, Department of Applied Physics, University of Groningen, Nyenborgh 4, 9747 AG Groningen, The Netherlands
[b] Current address: School of Mechanical, Materials and Energy Engineering, IIT Ropar, 140001, India

ARTICLE INFO

Article history:
Received 10 August 2014
Received in revised form 23 December 2014
Available online 2 February 2015

Keywords:
Discrete dislocation plasticity (DDP)
Rate sensitivity
Bulk behaviour
Yield stress
Obstacles

ABSTRACT

Discrete dislocation dynamics simulations are carried out to systematically investigate the rate dependent deformation behaviour of polycrystalline bulk copper by varying the loading rate in the range of 100–25,000 s^{-1} under tension. The underlying material model not only incorporates the realistic definition of nucleation time but also put emphasis on the role of obstacle density and their strength on dislocation motion. In the simulations, plasticity arises from the collective motion of discrete dislocations of edge character. Their dynamics is incorporated through constitutive rules for nucleation, glide, pinning and annihilation. The numerical results show that the rate sensitivity of yield stress in bulk polycrystals is controlled by the density of Frank-Read sources, obstacles and their strength.

1. Introduction

The plastic deformation of materials as a function of the applied loading rate has long been the subject of extensive research (e.g., Follansbee et al., 1984; Klopp et al., 1985; Clifton, 1990; Tong et al., 1992; Armstrong and Walley, 2008). The understanding of dynamic plastic behaviour of metals is important in many engineering applications including high speed machining, impact loading etc. Numerous experiments have demonstrated that the mechanical properties of materials such as yield stress and strength depend on the applied loading rate (Follansbee et al., 1984; Klopp et al., 1985; Rittel et al., 2002; Vural et al., 2003). It is generally observed that the flow stress slowly rises with strain rate at low rates, and increases more rapidly at strain rates $\dot{\varepsilon} > 10^3\ s^{-1}$ (Follansbee et al., 1984; Clifton, 1990; Tong et al., 1992). Based on the experimental findings of flow behaviour of aluminium and copper, Kumar et al. (1968), Kumar and Kumble (1969) have attributed this increase in flow stress to the different deformation mechanisms at low and high strain rates. In a similar study on copper, Follansbee et al. (1984) and Regazzoni et al. (1987) concluded that the deformation is controlled by thermal activation in low strain rate region ($\dot{\varepsilon} \leqslant 10^3\ s^{-1}$). In the high strain rate regime ($\dot{\varepsilon} \geqslant 10^4\ s^{-1}$), viscous drag was identified as the rate limiting mechanism. In another study, Frutschy and Clifton (1998) have shown that at high loading rates, the viscous resistance to dislocation motion not only governs the response of OFHC copper at room temperature but is important at elevated temperatures too.

Rate sensitivity is strongly material dependent and has been studied most intensively at the macroscopic scale within the context of superplasticity. Along with the identification of the mechanisms behind rate sensitivity, there has been much interest in constitutive models that include rate dependence. More recently, it has been found that the rate sensitivity depends on the grain size of the material, with values increasing for decreasing grain size (Hallberg et al., 2010). At these small grain sizes, there are size effects that cannot be captured by classical continuum plasticity models, as they lack a material length scale.

Discrete dislocation plasticity (DDP) is a modelling framework that is endowed with several length scales and has been shown to be able to quantitatively predict small-grain size plasticity of copper thin films (Shishvan and Van der Giessen, 2010). However, it has not been used

* Corresponding author.

http://dx.doi.org/10.1016/j.mechmat.2015.01.009
0167-6636/

yet, to study the complex rate dependent response of materials. In the context of probing the rate sensitivity of plastic flow, it is important to note that this DDP framework has two intrinsic time scales: one being the dislocation nucleation time t_{nuc} and the other given by the ratio of elastic modulus E and viscous drag B. This raises the question to what extent these two are capable of capturing the experimentally observed trends.

In order to answer this question, we perform DDP simulations of the tensile response of polycrystalline copper (Cu) as a function of strain rate. The effect of various parameters, such as viscous drag B, nucleation source density ρ_{nuc}, obstacle density ρ_{obs} and obstacle strength τ_{obs}, on the hardening behaviour of Cu is also investigated. The results are compared with experimental data from the literature.

2. DDP model

A polycrystalline bulk material under tension is modelled as a two-dimensional array of rectangular grains with height h and width d, as shown in Fig. 1. Each grain has three slip systems oriented 60° relative to each other, see Fig. 1(b). The orientation of each grain ϕ is different and is determined by random selection from a uniform distribution. Consistent with the plane strain conditions perpendicular to the plane of observation, only edge dislocations having Burgers vector b are used as carriers of plasticity. All grain boundaries (GBs) are assumed to be impenetrable for dislocations. Periodic boundary conditions are used across the simulation cell to prescribe the tensile strain ε. The top and bottom surface of the bulk are assumed to be traction free. The boundary conditions are imposed through the superposition method of Van der Giessen and Needleman (1995).

The analysis of the deformation process is performed in an incremental manner. After every update of the dislocation structure, the new driving force for the evolution of the structure is computed. This so-called Peach–Koehler force is determined by the applied stress and the long-range interactions of dislocations, which are accounted for by modelling them as line defects in a linear elastic solid. The driving force for the change in position of any dislocation is computed from superposition of the singular stress field of all other dislocations as if they were in infinite space and an image field that corrects for the actual boundary conditions, see Van der Giessen and Needleman (1995). The glide component of this force, f^I, controls the glide velocity v^I of dislocation I through the drag law $v^{(I)} = f^I/B$, where B is the drag coefficient.

While long-range interactions are taken into account by the elastic fields, a set of constitutive rules is used to incorporate the short ranged dislocation mechanisms that govern nucleation, annihilation and pinning of dislocations at obstacles. The Peach–Koehler force also controls the nucleation of dislocations through a two-dimensional (2d) version of the Frank-Read source, as proposed in Van der Giessen and Needleman (1995). According to this model, a dislocation dipole is generated when the resolved shear stress at a source exceeds its strength τ_{nuc} for a time span of t_{nuc}. The sign of the dipole is determined by the direction of the Peach–Koehler force. Following the source model of Shishvan and Van der Giessen (2010), the nucleation strength τ_{nuc} of the Frank-Read source contains two contributions,

$$\tau_{\text{nuc}} = \tau_{\text{nuc}}^{\text{LN}} + \tau_{\text{nuc}}^{0}. \tag{1}$$

The first term is a random value from a log-normal distribution that is determined by the grain size and the theoretical strength of the material. The second term, τ_{nuc}^{0}, is a material dependent parameter that accounts for the fact that a Frank-Read segment cannot always bow-out freely, but may interact with various types of obstacles such as small precipitates and forest dislocations. The mean effect of these size and position dependent obstacles to dislocation motion is incorporated by an offset value τ_{nuc}^{0}. It is considered a fit parameter to be obtained from comparison of simulation and experiments, as explained in the subsequent section.

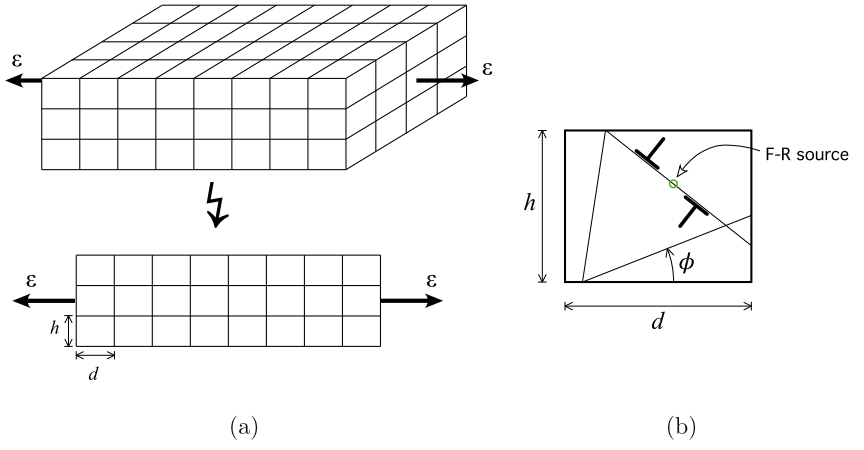

Fig. 1. (a) Two-dimensional representation of a polycrystal under tension and (b) plane strain model of single grain with slip systems and a source with dislocation dipole.

The nucleation time t_{nuc} used in Shishvan and Van der Giessen (2010) is defined as

$$t_{nuc} = \frac{\eta}{2}\frac{Bl_{FR}}{\tau_{nuc} b}\mathcal{F}(\zeta), \tag{2}$$

where η depends on the line character (e.g. for an initially edge dislocation source $\eta = 1.5$), $\zeta = \tau/\tau_{nuc}$ and $\mathcal{F}(\zeta)$ is a rapidly decaying function with a singularity at the threshold stress, i.e. $\tau = \tau_{nuc}$. The parameter l_{FR} in this expression is the length of the Frank-Read segment in three dimensions before it bows out and is for each source computed from its strength τ_{nuc} using the line tension approximation

$$\tau_{nuc} = \beta_{nuc}\frac{\mu b}{l_{FR}} \quad \text{with} \quad \beta_{nuc} = \frac{1}{2\pi}\left(\ln\frac{l_{FR}}{b} + 0.5\right),$$

in an iterative manner. The value of t_{nuc} according to Eq. (2) is an estimate by Benzerga (2008) of the time needed to achieve the bowed-out configuration labelled config1 in Fig. 2(a). In reality, the dislocation needs to further grow to config2 (see Fig. 2(a)) before forming a complete, new dislocation loop. Three-dimensional simulations in Shishvan et al. (2008) have shown that the time to reach config2 is larger than the time to attain config1. In the present approach, therefore, the time elapsed to reach config2 (i.e., the actual nucleation time) is calculated by multiplying the t_{nuc} with an enhancement factor η (see Fig. 2(b)) which is obtained by fitting the simulation data of Shishvan et al., 2008.

It is worth noting here that, as the actual nucleation times among random sources during a simulation turned out to vary widely, it was necessary to introduce an adaptive time stepping scheme that captures all nucleation events. This is achieved by choosing the incremental time step dt equal to the minimum nucleation time among all activated sources at any instant.

Annihilation of two edge dislocations having equal and opposite Burgers vector occurs when they are brought sufficiently close together. This is modelled by removing two dislocations when they are within a material-dependent, critical annihilation distance $L_e = 6b$.

In real materials, the motion of dislocation along the slip plane can be hindered by several types of obstacles, such as small precipitates, clusters, forest dislocations on intersecting slip planes etc. These are explicitly incorporated in the current 2d-DDP model as point obstacles at which moving dislocations get pinned (Van der Giessen and Needleman, 1995). These pinned dislocations are the origin of dislocation pile-ups. The stress acting on the leading dislocation increases with the increasing number of dislocations in pile-up. Once the resolved shear stress on leading dislocation exceeds the obstacle's strength τ_{obs}, it is released and allowed to move past obstacle. Grain boundaries are treated as impenetrable obstacles. Inside dislocation pile-ups, the position of dislocations is quite unstable and they tend to have high velocity oscillatory motions (Cleveringa et al., 1999). To reduce these irrelevant vibrations, the shear wave speed is used as a cut-off for the dislocation velocity. All other details of the DDP model can be found in Shishvan and Van der Giessen (2010).

3. DDP modelling of rate effects in bulk materials

The tensile response of a bulk polycrystalline material is modelled by using three layers of eight grains, cf. Fig. 1. This choice is motivated by previous DDP computations on single and multiple layer films in tension, which have revealed that free-surface effects can be neglected from three layers onwards (Kumar et al., 2009) and that eight grains is sufficient for a statistically meaningful average response (Shishvan and Van der Giessen, 2010). The grains are taken to have an aspect ratio of $h/d = 0.67$. Each grain has three slip systems, with a spacing of $200b$ between parallel slip planes. Dislocation sources having a log-normally distributed strength are randomly distributed among the grains and randomly positioned on the slip planes with a density ρ_{nuc}. In some computations we study

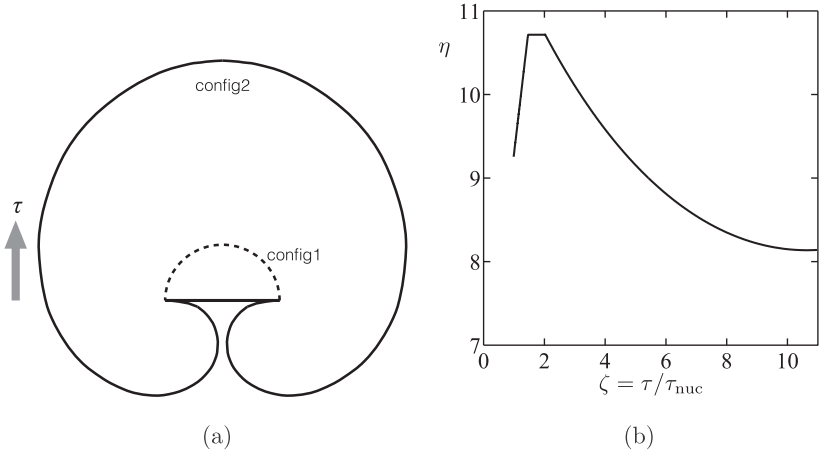

Fig. 2. (a) Configurations used to define the nucleation time t_{nuc} and (b) variation of the ratio η between the times to reach config2 and config1 in (a) as a function of non-dimensional stress $\zeta = \tau/\tau_{nuc}$. This ratio is used as an enhancement factor of the nucleation time in the present 2d-DD simulations.

the effect of obstacles that have the same strength τ_{obs} and are randomly distributed over the slip planes with an obstacle density ρ_{obs} (in fact, they are placed only on planes that have at least one source to ensure that each obstacle has the potential opportunity to interact with dislocations).

In the remainder of this study we will have Cu in mind, since Shishvan and Van der Giessen (2010) have shown that the predictions of the tensile response of columnar Cu films using the DDP method above are in quantitative agreement with experimental results of Xiang and Vlassak (2006) for a range of grain sizes and film thickness. These previous simulations adopted the following characteristic material parameters: $E = 110$ GPa, $\nu = 0.34$, $b = 0.25$ nm and $B = 10^{-4}$ Pa s. Assuming that those thin films were obstacle free after sputtering (Xiang and Vlassak, 2006), the model contains only two unknown material parameters: source density and source strength. In Shishvan and Van der Giessen (2010), these source properties were fitted to the experimental results of films with a particular thickness and grain size; using these values, the behaviour of films with different thickness and grain size was predicted with notable accuracy. Xiang and Vlassak (2006) have also prepared and analysed films that were passivated and showed that these passivation layers prevented dislocations from escaping the crystals. As far as the dislocation evolution is concerned, the effect of passivation layers is similar to that of impenetrable grain boundaries. Thus, we use the experimental data for passivated films with $h = 1$ μm and $d = 1.5$ μm as input to determine the source properties of the bulk polycrystalline material that we want to study. Following the same procedure as in Shishvan and Van der Giessen (2010), we obtain $\rho_{nuc} = 30\ \mu m^{-2}$ and $\tau^0_{nuc} = 34.5$ MPa. This value of τ^0_{nuc} will be used throughout this study, except when the effect of source density is studied in one of the forthcoming sections. In view of the way the thin films in Xiang and Vlassak (2006) were produced, it is assumed here, like in Shishvan and Van der Giessen (2010) that there are no obstacles.

Loading is prescribed in terms of a constant value of $\dot{\varepsilon}$ and the required tensile stress σ is computed in time as a function of $\varepsilon = \int \dot{\varepsilon} dt$. In order to reduce the inevitable stochasticity in a finite-cell computation caused by the random grain orientations and the random positions and strengths of the sources, an average of 5 realizations is used for each strain rate. The standard deviation among various realizations is shown as an error bar.

4. Model prediction and comparison with experiments

We start out by considering the predicted stress–strain curves. Fig. 3(a) reveals that upon varying the strain rate by several orders of magnitude (100–25,000 s^{-1}), the plastic branch of the stress–strain curve shifts up but hardly changes shape. The origin of this shift is revealed by Fig. 3(b), showing the dependence of stress σ on the evolving dislocation density ρ. The first thing to observe is that the stress level at which the first dislocations are being generated, σ_{nuc}, increases with strain rate. The origin of this is that it takes time to nucleate a dislocation dipole: once the activation of a source is initiated, at the macroscopic stress level σ_{in}, it takes a time t_{nuc} before the dislocations are actually generated. During this time interval, the elastic strain increases by $\dot{\varepsilon} t_{nuc}$, thus leading to the connection

$$\sigma_{nuc} = \sigma_{in} + E^* \dot{\varepsilon} t_{nuc}. \tag{3}$$

To elucidate this argument, the stress levels σ_{in} and σ_{nuc} are marked in Fig. 3(b) for $\dot{\varepsilon} = 2500\ s^{-1}$, as an example. Since the initiation stress σ_{in} depends only on the source distribution, the expression (3) provides a first and important clue for the rate sensitivity in DDP simulations. It is noted that the plane-strain elastic modulus $E^* = E/(1-\nu^2)$ appears in (3) just because our 2d analysis is in plane strain, yet this is readily generalised.

The importance of the generation of dislocations in setting the rate sensitivity is further elucidated by Fig. 4 showing the evolution of the dislocation density ρ during tension. Contrary to the stress response, the evolution of the dislocation density is much less sensitive to the strain rate $\dot{\varepsilon}$. Fig. 4(a) shows that the main difference in the evolution of ρ for different $\dot{\varepsilon}$ is that the generation of dislocation is delayed at increasing strain rates. As a result, all curves corresponding to different $\dot{\varepsilon}$ fall on top of each other in Fig. 4(b) when plotting the dislocation density ρ as function of "plastic" strain $\varepsilon - \varepsilon_{nuc}$.

Since strain rate appears to affect initial yield much more than strain hardening, we focus attention now on the yield strength σ_Y, defined here at 0.1% offset strain (see Fig. 3(a)). The values predicted by DDP are plotted against strain rate in Fig. 5(a) (solid line, filled circles). Interestingly, the dependence of σ_Y on $\dot{\varepsilon}$ appears to have two distinct regions. In the first region, of strain rates $\dot{\varepsilon} < 2500\ s^{-1}$, the yield strength is only weakly dependent on the strain rate $\dot{\varepsilon}$, whereas in the regime of higher strain rates, the yield strength grows more rapidly.

Next, Fig. 5(b) confronts our DDP predictions with experimental results on the strain rate dependent flow stress of OFHC copper from two different sources, Follansbee et al. (1984) and Tong et al. (1992) (Cu is used for benchmarking since this is what the material parameters were fitted for). To put the study in even broader context, also the results for Al obtained in Klopp et al. (1985) are included. Even though the actual stress levels are different, the trends in rate dependence are very similar, thus suggesting that they may be rather universal for FCC materials (cf., Zerilli and Armstrong, 1992).

The difference in the predicted yield strengths from the experimental data of OFHC copper (Follansbee et al., 1984; Tong et al., 1992) may have various origins. One reason is that the DDP yield strength is defined at 0.1% plastic strain whereas the experimental values are taken at much higher strains of 15%. Another contribution may be that the material dependent model parameter τ^0_{nuc} has been fitted to the experimental results of Xiang and Vlassak (2006) on thin films with grain sizes on the order of micrometers which were manufactured by electroplating or sputter deposition. This value may therefore not be representative for bulk Cu as studied in Follansbee et al. (1984) and Tong et al. (1992).

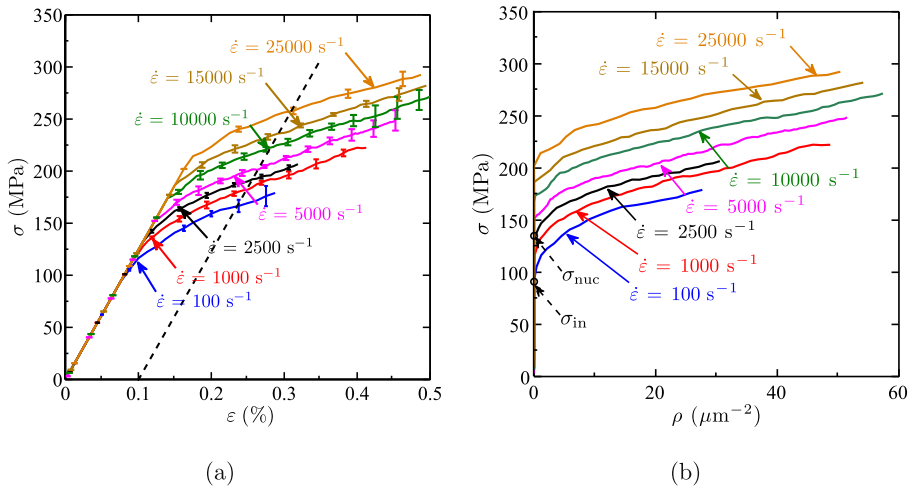

Fig. 3. Effect of strain rate $\dot{\varepsilon}$ on (a) the evolution of average stress σ with strain ε and (b) dislocation density ρ in bulk Cu for the default parameter values specified in Section 3.

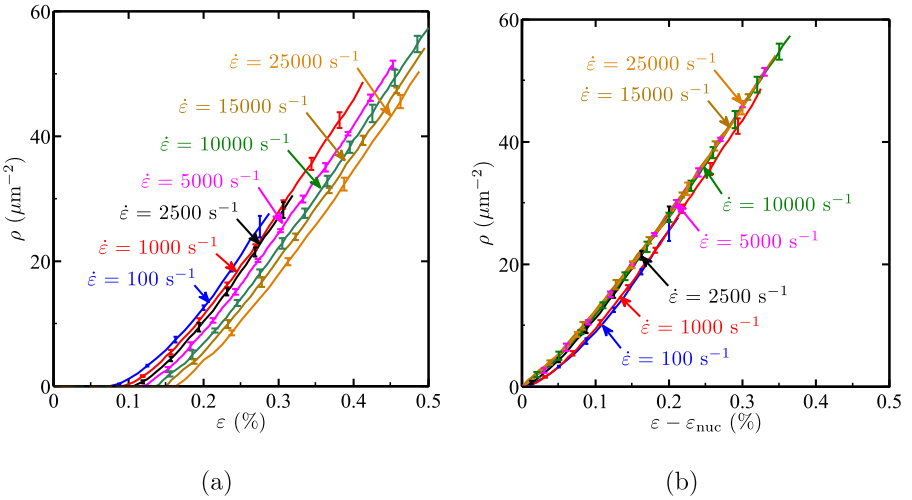

Fig. 4. Evolution of average dislocation density ρ with (a) strain ε and (b) plastic strain $\varepsilon - \varepsilon_{nuc}$. The parameter ε_{nuc} is defined as the strain corresponding to first dislocation nucleation in all cases for bulk Cu with $\rho_{nuc} = 30\ \mu m^{-2}$.

As a check for the above argument and to show the predictive capabilities of the DDP framework, Fig. 5(b) shows that we are able to match the experimental results for OFHC copper (Follansbee et al., 1984) by using $\tau^0_{nuc} = 63.5$ MPa ($\diamondsuit$ symbols on top of the experimental data of Follansbee et al. (1984)).

The two regimes in rate dependence of the yield (or flow) stress observed in Fig. 5 become even more distinct when studying the strain rate sensitivity parameter m defined by

$$m = \frac{\partial \log \sigma_Y}{\partial \log \dot{\varepsilon}}. \tag{4}$$

As shown in Fig. 6 the DDP results reveal that $m = 0.045$ in the lower strain rate regime of $\dot{\varepsilon} \leqslant 2500\ s^{-1}$, and that it steeply increases up to $m = 0.17$ when $\dot{\varepsilon} \approx 10,000\ s^{-1}$. The experimental results for bulk Cu and Al included in Fig. 6 show a similar trend with a somewhat lower m in the region of $\dot{\varepsilon} \leqslant 2500\ s^{-1}$ and higher value of m when $\dot{\varepsilon} \geqslant 10,000\ s^{-1}$. The DDP simulations have not been run at strain rates below 100 s^{-1} for they would take very long computing times without giving any new insight. The rate dependence in this regime is still nucleation-controlled according to Eq. (3) and the rate value of m is not expected to change much. Experimentally, the rate dependence at $10^{-3}\ s^{-1} \leqslant \dot{\varepsilon} \leqslant 10^2\ s^{-1}$ is the same as for the range 10^2 to $10^3\ s^{-1}$ as plotted in Fig. 6, but is commonly attributed to thermally activated processes for a dislocations to pass obstacles such as precipitates, forest dislocations, impurity atoms, etc. (Follansbee et al., 1984).

The increased yield stress or rate sensitivity m in the region $\dot{\varepsilon} > 5000\ s^{-1}$ has previously been attributed to a

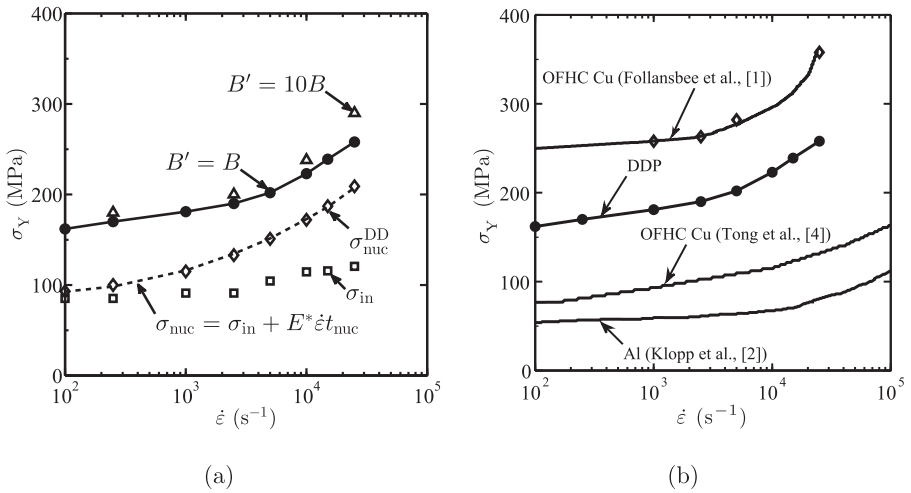

Fig. 5. Strain rate dependence of yield strength σ_Y. (a) DDP predictions (solid dots), including the partitioning of the rate effects due to dislocation generation and glide (indicated with □, ◇ and △). (b) Comparison of the predictions using our default and a set of modified input parameters (solid dots and ◇, respectively) with experimental results for OFHC copper (Follansbee et al., 1984; Tong et al., 1992) and for Al (Klopp et al., 1985).

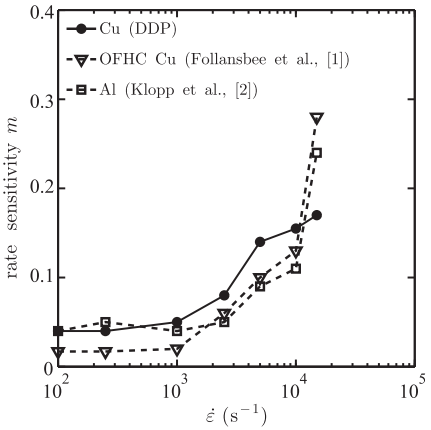

Fig. 6. Strain rate sensitivity m as a function of applied strain rate $\dot{\varepsilon}$ from DDP computations along with the experimental data for OFHC copper (Follansbee et al., 1984) and Al (Klopp et al., 1985).

change in controlling deformation mechanism as we move from low to very high strain rates (Kumar and Kumble, 1969; Frost and Ashby, 1971; Follansbee et al., 1984; Regazzoni et al., 1987; Zerilli and Armstrong, 1992). At these high strain rates the stress acting on dislocations is so large that it can easily pass through the obstacles and dislocation glide is controlled by the viscous drag mechanisms inside the material. The latter is verified here by repeating some of the simulations with a ten times higher drag coefficient B in the glide motion (note that the influence of B on the nucleation time through Eq. (2) was deliberately excluded in order to separate the contributions from nucleation and glide). Fig. 5(a) shows that the yield strength σ_Y is barely affected when using the higher B (open △'s) in the low strain rate region. On the other hand, the predicted yield strength is significantly higher in the high strain rate region, thus confirming that indeed yield in the high strain rate region is dominated by drag (Frost and Ashby, 1971; Johnson and Tonks, 1991; Zerilli and Armstrong, 1992).

5. Parameter study

The density of sources and obstacles, as well as their strength, are key parameters in the model. As discussed in Section 3, the parameters used so far were fitted to experimental results on passivated thin films (Xiang and Vlassak, 2006), similar to those used in Shishvan and Van der Giessen (2010) for free-standing thin films. We now proceed with investigating the effect on rate sensitivity of source density, obstacle density and their strength through a parametric study. This will not only give more insight into the physical origin of rate sensitivity, it may also provide hints for tailoring the rate dependent response of materials by modification of their microstructure.

5.1. Effect of obstacles

By having assumed, so far, that crystals are free of obstacles, the rate dependence of plasticity is determined by the time scale of generating new dislocations and by the time to traverse the distance to the grain boundaries (which are impenetrable). Real materials may have a variety of different agents that serve as obstacles to dislocation motion, such as small precipitates and forest dislocations. In order to investigate their role, we repeat the simulations by varying the density ρ_{obs} of randomly positioned point obstacles with a certain strength while retaining the properties of the sources. Fig. 7 reveals that the yield stress increases monotonically with increasing ρ_{obs}. However, the strengthening due to the presence of obstacles decreases at higher loading rates. Experimental evidence of such weaker rate sensitivity at high strain rates caused by the presence of impurities in Al and Cu alloys has been reported in Klopp et al. (1985).

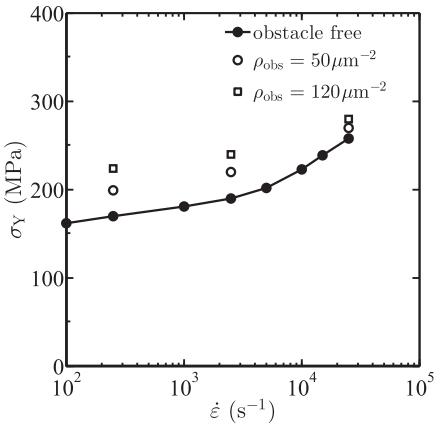

Fig. 7. Effect of obstacle density ρ_{obs} on the rate dependent yield strength σ_Y with $\rho_{nuc} = 30\ \mu m^{-2}$ and $\tau_{obs} = 112$ MPa. The obstacle free case with $\rho_{nuc} = 30\ \mu m^{-2}$ is the one presented in Figs. 3–5.

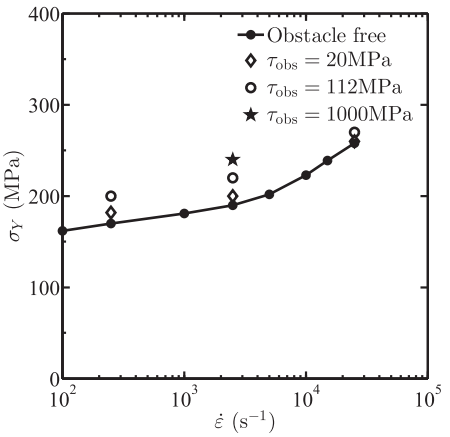

Fig. 8. Effect of obstacle strength τ_{obs} on the rate dependent yield strength σ_Y with with $\rho_{nuc} = 30\ \mu m^{-2}$ and $\rho_{obs} = 50\ \mu m^{-2}$. The baseline curve corresponding to the obstacle free case is included for comparison purpose.

The increase in obstacle density not only increases the probability for a dislocation to get pinned, it also reduces the average dislocation velocity as the mean-free path of a dislocation depends linearly on obstacle spacing. This causes a reduction in plastic strain rate, as is evident from Orowan's law for the plastic strain rate: $\dot{\varepsilon}^p = \rho b v$, with ρ the dislocation density and v the mean dislocation velocity. Hence, the number of obstacles and their spacing is strongly felt and we see a significant increase in yield stress in the region $\dot{\varepsilon} \leqslant 2500\ s^{-1}$. However, in the high strain rate region, when the applied stress is sufficiently high, dislocations are able to easily bypass the obstacles. Once they overcome these barriers, the presence of obstacles does not contribute much to the strengthening of the material. Consequently, in the regime $\dot{\varepsilon} \geqslant 10,000\ s^{-1}$, we observe a smaller increase in σ_Y with ρ_{obs}.

For the same reason, the influence of the strength of the obstacles diminishes at higher strain rates, as is shown in Fig. 8. The change in yield stress when increasing τ_{obs} from 20 to 112 MPa is as large as when increasing it by an order of magnitude to $\tau_{obs} = 1000$ MPa.

5.2. Dependence on source density

The results presented in the previous section were for a source density of $\rho_{nuc} = 30\ \mu m^{-2}$. In this subsection we vary the number of Frank-Read sources initially present in the grains such that the source density ρ_{nuc} ranges from 20 to 50 μm^{-2}. Fig. 9(a) shows that an increase in ρ_{nuc} shifts the yield stress vs strain rate curve down by a constant amount and does not significantly alter the sensitivity of σ_Y on $\dot{\varepsilon}$. This implies that the rate sensitivity parameter predicted by DDP is independent of source density within the range studied here.

The variation in ρ_{nuc} has a similarly small effect on the rate dependence when obstacles are present in the sample, as shown in Fig. 9(b), even though the presence of obstacles significantly increases the yield strength of the material.

5.3. Effect of grain size

To gain some insight in the effect of grain size on the rate dependent yield stress, Fig. 10 augments the findings for the default grain size of $d = 1.5\ \mu m$ with results for $d = 2\ \mu m$. The grain aspect ratio h/d is kept constant at 0.67 and all material parameters are the same as in Section 4. As expected Shishvan and Van der Giessen (2010), an increase in grain size reduces the value of σ_Y. However, the change in grain size does not affect the rate sensitivity of yield stress as is evident from the fact that the slope of the σ_Y vs $\dot{\varepsilon}$ curve is the same in both cases. The lower yield stress in bigger grains can be a consequence of several factors such as available dislocation glide distance, reduced piling-up of dislocations against grain boundaries and size-dependent source strength distribution, as explained in Nicola et al. (2003); Nicola et al., 2005, Kumar et al. (2009), Shishvan and Van der Giessen (2010).

6. Discussion of power law viscoplasticity

The definition (4) corresponds to the power law relation

$$\frac{\sigma_Y}{\sigma_0} = \left(\frac{\dot{\varepsilon}}{\dot{\varepsilon}_0}\right)^m \tag{5}$$

with reference stress and strain rate σ_0 and ε_0, respectively. This is a convenient relationship when thinking about rate dependence, but it is important to note that the strain-rate dependence of the yield stress found experimentally (at room temperature) as well as from DD simulations does not obey (5), as this would imply that the value of m computed from Fig. 5(b) is a constant for each material, which is clearly not the case according to Fig. 6. Instead, Fig. 5(a) suggests linear relations between yield strength and logarithm of strain-rate: one at low strain rate ($\dot{\varepsilon} \lessapprox 5 \times 10^{-3}\ s^{-1}$) and one at high strain rate. The cross-over between both regimes appears to occur at roughly the same strain rate for all FCC materials shown

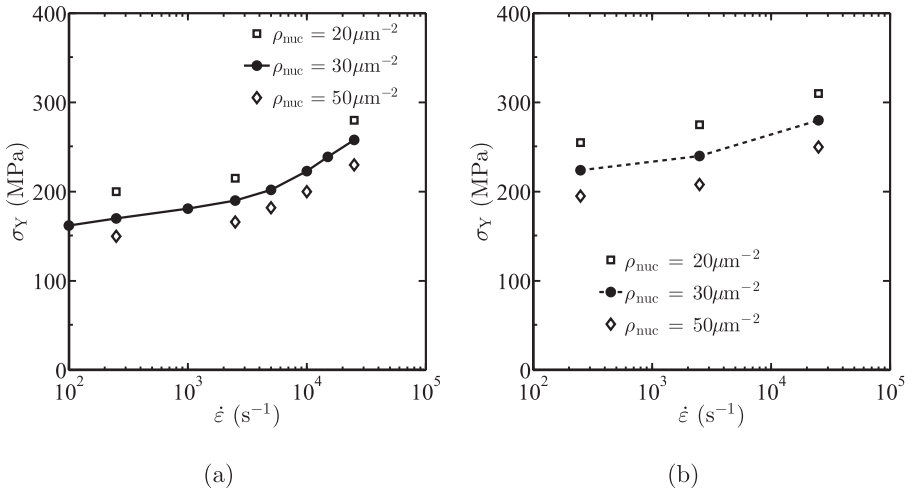

Fig. 9. Effect of source density $\rho_{\rm nuc}$ on the rate dependent yield strength $\sigma_{\rm Y}$ (a) when the material is obstacle free and (b) with $\rho_{\rm obs} = 120\ \mu{\rm m}^{-2}$ and $\tau_{\rm obs} = 112$ MPa (cf., Fig. 8).

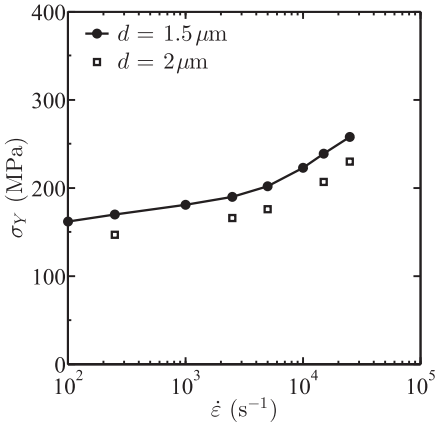

Fig. 10. Effect of grain size on the rate dependent yield strength $\sigma_{\rm Y}$ of an obstacle free material with $\rho_{\rm nuc} = 30\ \mu{\rm m}^{-2}$.

in Figs. 5 and 6, and at a somewhat lower strain rate in steels (Vural et al., 2003). A linear relation between $\sigma_{\rm Y}$ and $\log\dot{\varepsilon}$ is consistent with the phenomenological Ludwik model (Ludwik, 1909) as well as with the relation proposed by Klepaczko and Chiem (1986) based on dislocation physics. It is interesting to note, though, that the latter attributes rate sensitivity to thermally activated motion of dislocations over obstacles and to dynamic recovery associated with the collision and annihilation of dislocations. Even though dynamic recovery in this sense is not accounted for in our DDP model, our DD predictions are consistent with experimental trends.

The expression (5) looks similar to the popular viscoplastic power law

$$\frac{\sigma}{\sigma_{\rm Y}} = \left(\frac{\dot{\varepsilon}^{\rm p}}{\dot{\varepsilon}^{\rm p}_0}\right)^M \quad \text{or} \quad \frac{\dot{\varepsilon}^{\rm p}}{\dot{\varepsilon}^{\rm p}_0} = \left(\frac{\sigma}{\sigma_{\rm Y}}\right)^{1/M}, \tag{6}$$

describing the dependence of the plastic strain rate $\dot{\varepsilon}^{\rm p}$ on the current stress level σ, yet is quite different at the same time (which is why the exponent in (6) is called M instead of m). While (5) governs the dependence of the yield strength (or flow strength at 0.1% strain) on the applied strain rate, the viscoplastic law (6)b gives the instantaneous *plastic* strain rate at the current stress level in a material with flow strength $\sigma_{\rm Y}$. The viscoplastic law (6)b is a useful description of Norton creep at high temperature, and it is conveniently used in computational plasticity as an alternative to the yield condition: $\dot{\varepsilon}^{\rm p} \leqslant 0$ when $\sigma = \sigma_{\rm Y}$ (to keep the argument simple, we here assume tension, not compression which would just make the signs change).

It is instructive to consider the consequences of Eq. (6)b in a tensile test at constant strain rate. Within the framework of classical plasticity, based on the decomposition of strain into elastic and plastic parts $\varepsilon = \varepsilon^{\rm e} + \varepsilon^{\rm p}$, Hooke's law for the elastic response, $\sigma = E\varepsilon^{\rm e}$, gives the evolution equation $\dot{\sigma} = E(\dot{\varepsilon} - \dot{\varepsilon}^{\rm p})$. Under constant strain rate, $\dot{\varepsilon}$ can be factored out and the instantaneous tangent modulus $E_{\rm T} = d\sigma/d\varepsilon$ can be written as

$$E_{\rm T} = E\left(1 - \frac{\dot{\varepsilon}^{\rm p}}{\dot{\varepsilon}}\right),$$

where the right-hand side is a function of σ through Eq. (6). When we evaluate $E_{\rm T}$ at the moment that $\sigma = \sigma_{\rm Y}$, we obtain

$$\frac{E_{\rm T,Y}}{E} = 1 - \frac{\dot{\varepsilon}^{\rm p}_0}{\dot{\varepsilon}}, \tag{7}$$

which is a constant. This analysis continues to hold when $\sigma_{\rm Y}$ is not the initial (or 0.1%) yield strength but the flow strength at some level of plastic strain. Thus, we find that the viscoplastic power law implies that the material responds to increasing applied strain rates by enhancing its hardening rate. As in this point of view there is no information about the effect of strain rate on $\sigma_{\rm Y}$ itself, we would recover a description of what Klepaczko and Chiem Klepaczko and Chiem, 1986 called "rate sensitive strain hardening", see their Fig. 16b.

However, our DD show no rate dependence of hardening, see 3(a), but only of yield (so-called "instantaneous rate sensitivity", cf. Fig. 16a in Klepaczko and Chiem (1986)). If we want to capture this behaviour by the viscoplastic framework, we have to conclude that $\dot{\varepsilon}_0^{\mathrm{p}}$ must depend on strain rate in such a way that $E_{\mathrm{T,Y}}/E$ is rate independent. According to (7) this would require $\dot{\varepsilon}_0^{\mathrm{p}} \propto \dot{\varepsilon}$, which according to (6)b would imply that $\dot{\varepsilon}^{\mathrm{p}} \propto \dot{\varepsilon}$. But then, this means that, effectively, the response is not viscoplastic in the sense that the plastic deformation is autonomous and determined instantaneously by the current stress level; instead, the plastic strain rate follows the applied strain rate, just like in rate-independent plasticity theories. The only rate dependence that persists is the rate sensitivity of the intrinsic properties $\dot{\varepsilon}_0^{\mathrm{p}}$ and σ_{Y}.

This finding is intimately connected to the observation in Fig. 4(b) that dislocation density is independent of strain rate. We can rationalise this by starting from the assumption that the dislocation density ρ is a function of plastic strain and plastic strain rate: $\rho = \rho(\varepsilon^{\mathrm{p}}, \dot{\varepsilon}^{\mathrm{p}})$. Then, the rate of change of ρ at any given ε^{p} would have a contribution depending on the rate of change of $\dot{\varepsilon}^{\mathrm{p}}$. However, as shown above, instantaneous rate sensitivity implies that E_{T}/E is independent of strain rate and therefore that $\dot{\varepsilon}^{\mathrm{p}} \propto \dot{\varepsilon}$. Hence, during a *constant* strain rate test, $\dot{\varepsilon}^{\mathrm{p}}$ is constant and the dislocation density only changes according to

$$\dot{\rho} = \frac{\partial \rho}{\partial \varepsilon^{\mathrm{p}}} \dot{\varepsilon}^{\mathrm{p}}.$$

This is the same as when the dislocation density ρ were given by $\rho = \rho(\varepsilon^{\mathrm{p}})$, which is essentially what is shown in Fig. 4(b).

7. Conclusion

We have investigated the rate dependent tensile behaviour of a polycrystalline bulk FCC material by means of two-dimensional discrete dislocation plasticity. This computational framework aims at low-temperature and small strain plasticity and only incorporates dislocation generation and glide. Rate sensitivity originates from two constitutive rules that involve a time scale: nucleation of dislocations by a Frank-Read mechanism and glide governed by linear drag. The computations reveal that these simple explicit rate dependencies give rise to more complex, nonlinear strain rate sensitivity as a consequence of the collective behaviour of dislocations, and their interaction with grain boundaries and other obstacles.

The salient conclusions of this study are:

- Discrete dislocation plasticity gives rise to instantaneous rate sensitivity. With the constitutive rules used here, the hardening rate is independent of strain rate.
- The value of the rate dependent yield strength σ_{Y} and of the rate sensitivity parameter m rise rather quickly beyond a strain rate of around $5000\,\mathrm{s}^{-1}$. This is consistent with experimental findings for simple FCC materials such as Cu and Al.
- The upturn in rate sensitivity is due to the change in dominating deformation mechanism. While in the low strain rate region $\dot{\varepsilon} \leqslant 2500\,\mathrm{s}^{-1}$ plastic deformation is primarily controlled by dislocation production and their motion past obstacles, plasticity is controlled by viscous dissipation at strain rates $\dot{\varepsilon} \geqslant 10,000\,\mathrm{s}^{-1}$.
- A parametric study has revealed that the rate sensitivity can be modified to a certain extent by varying the obstacle density and obstacle strength, while the source density has a negligible influence. Moreover, for grain sizes in the micrometer regimes, grain size does have a strong effect on the yield strength but not on its rate sensitivity.

From a materials science point of view, the agreement of the predicted instantaneous rate sensitivity with experimental observations (cf. Fig. 6) seems remarkable in view of the simplicity of the model. A bulk polycrystalline material is represented by a two-dimensional array of rectangular grains, containing edge dislocations only, while many dislocation mechanisms are not included explicitly. Among the lacking dislocation mechanisms are intrinsically three-dimensional phenomena such as the formation of strong dislocation locks, and the dynamic formation and destruction of Frank-Read sources, but we expect that these may be more important for the rate sensitivity of hardening than for yield. However, relaxation mechanisms such as cross-slip and dynamic recovery are not taken into account explicitly. Yet in so far as these may be affecting the rate sensitivity of yield, their effects can be regarded to be incorporated indirectly through the effective glide mobility in the two-dimensional model. While this will restrict the model predictions to remain qualitative, and not be quantitatively predictive, it appears that the model contains the essential physics behind the rate sensitivity of polycrystalline metals at room temperature. It should be noted though that the model is isothermal and does not include thermally activated mechanisms which may shift the relative time scales of dislocation generation versus mobility.

It also bears emphasis that the strain rates studied here are at the high end of experimental tensile testing. A standard tensile test is typically carried out at strain rates that are several orders of magnitude lower, e.g. down to $\dot{\varepsilon} \approx 10^{-3}\,\mathrm{s}^{-1}$. At these low strain rates, dislocations glide past obstacles by thermally activated mechanisms and hence the residence or waiting time of a dislocation at individual obstacles may become the rate limiting factor (Frost and Ashby, 1971; Regazzoni et al., 1987). On the other hand, Follansbee et al. (1984) have pointed out that thermally-activated interactions between dislocations control the rate sensitivity only as long as the structure remains unchanged; that is, without the nucleation of dislocations. Thus, we expect that our observation that the rate sensitivity at low strain rates is controlled by dislocation nucleation will persist down to even lower strain rates than studied here, except when the density of mobile dislocations is so high that nucleation does not occur.

Acknowledgment

This research was financially supported by the Dutch Technology Foundation (STW), project 10108.

References

Armstrong, R.W., Walley, S.M., 2008. Int. Mater. Rev. 53 (3), 105–128.
Benzerga, A., 2008. Int. J. Plast. 24 (7), 1128–1157.
Cleveringa, H., Van der Giessen, E., Needleman, A., 1999. Int. J. Plast. 15 (8), 837–868.
Clifton, R.J., 1990. Appl. Mech. Rev. 43, S9–S22.
Follansbee, P.S., Regazzoni, G., Kocks, U.F., 1984. Inst. Phys. Conf. Ser. 70, 71–80.
Frost, H.J., Ashby, M.F., 1971. J. Appl. Phys. 42 (13), 5273–5279.
Frutschy, K., Clifton, R., 1998. J. Mech. Phys. Solids 46 (10), 1723–1744.
Hallberg, H., Wallin, M., Ristinmaa, M., 2010. Mater. Sci. Eng. A 527 (45), 1126–1134.
Johnson, J.N., Tonks, D.L., 1991. American Physical Society (APS) conference on shock compression of condensed matter, Williamsburg, VA, USA, 1991, pp. 371–378.
Klepaczko, J.R., Chiem, C.Y., 1986. J. Mech. Phys. Solids 34 (1), 29–54.
Klopp, R.W., Clifton, R.J., Shawki, T.G., 1985. Mech. Mater. 4 (34), 375–385.
Kumar, A., Kumble, R.G., 1969. J. Appl. Phys. 40 (9), 3475–3480.
Kumar, A., Hauser, F., Dorn, J., 1968. Acta Metall. 16 (9), 1189–1197.
Kumar, R., Nicola, L., Van der Giessen, E., 2009. Mater. Sci. Eng. A 527, 7–15.
Ludwik, P., 1909. Elemente der Technologischen Mechanik, Berlin.
Nicola, L., Van der Giessen, E., Needleman, A., 2003. J. Appl. Phys. 93 (10), 5920–5928.
Nicola, L., Van der Giessen, E., Needleman, A., 2005. Thin Solid Films 479 (12), 329–338.
Regazzoni, G., Kocks, U., Follansbee, P., 1987. Acta Metall. 35 (12), 2865–2875.
Rittel, D., Ravichandran, G., Lee, S., 2002. Mech. Mater. 34 (10), 627–642.
Shishvan, S.S., Van der Giessen, E., 2010. J. Mech. Phys. Solids 58 (5), 678–695.
Shishvan, S.S., Mohammadi, S., Rahimian, M., 2008. Model. Simul. Mater. Sci. Eng. 16 (7), 075002–17.
Tong, W., Clifton, R.J., Huang, S., 1992. J. Mech. Phys. Solids 40 (6), 1251–1294.
Van der Giessen, E., Needleman, A., 1995. Model. Simul. Mater. Sci. Eng. 3 (5), 689–735.
Vural, M., Ravichandran, G., Rittel, D., 2003. Metall. Mater. Trans. A 34, 2873–2885.
Xiang, Y., Vlassak, J.J., 2006. Acta Mater. 54 (20), 5449–5460.
Zerilli, F., Armstrong, R., 1992. Acta Metall. Mater. 40 (8), 1803–1808.